arXiv:1508.05998v1 [cond-mat.mes-hall] 24 Aug 2015

Spin relaxation in hole-doped transition metal dichalcogenide monolayer and bilayer with the crystal defects

Tetsuro Habe and Mikito Koshino
Department of Physics, Tohoku University, Sendai 980-8578, Japan
(Dated: August 26, 2015)

We study the electronic spin relaxation effect in the hole-doped monolayer and bilayer transition-metal dichalcogenides in the presence of the crystal defects. We consider realistic models of the lattice vacancy and actually estimate the spin relaxation rate using the multi-orbital tight-binding model. In the monolayer, the spin-relaxation time is found to be extremely long compared to the momentum relaxation time, and this is attributed to the fact that the spin hybridization in the band structure is suppressed by the mirror reflection symmetry. The bilayer TMD has a much shorter spin relaxation time in contrast, and this is attributed to stronger spin hybridization due to the absence of the mirror symmetry.

PACS numbers: 72.25.Dc,73.63.Bd,85.35.Ds

Monolayer transition-metal dichalcogenide(TMD) is a atomically thin two-dimensional semiconductor with a strong spin-orbit interaction[1]. In the electronic band structure, the spin and valley (K and K') degrees of freedom are intercorrelated because of the broken inversion symmetry in the atomic configuration, implying various spin-dependent phenomena and potential applications to the spintronic devices[1–9] and electronics[10–16].

While the spin-orbit interaction is a key to control the electronic spin, it also causes the spin relaxation at the same time in presence of the impurity scattering. In the conventional semiconductors, the spin polarization of the conduction electron rapidly decays in various processes such as Dyakonov-Perel mechanism and Elliott-Yafet mechanism.[17–20] In the TMDs, on the other hand, the recent experiment showed that the carriers in the valence bands have a relatively long spin-relaxation time compared to conventional materials[21]. The long spin life time comes from the peculiar band structure of TMD, where the spin-up and spin-down subbands split in opposite direction between K and K' valleys with a relatively large splitting width of the order of 100 meV [Fig. 1]. In the moderate hole concentration, therefore, the carriers at K and K' are fully polarized to opposite spin directions, and then the inter-valley scattering is necessary for the spin relaxation.

In this paper, we study the inter-valley spin relaxation effect caused by the non-magnetic short-range scatterers in hole-doped monolayer and bilayer TMDs. In the literature, the spin-relaxation in monolayer TMD was theoretically investigated for the conduction / valence bands and various different relaxation mechanisms.[22–26] The spin relaxation by the inter-valley scattering has also been discussed using effective impurity models,[26,27] while the spin-flip mechanism in actual crystal defect or impurity in the lattice structure has not been studied well. In what follows, we consider specific atomic defects[28] shown in Fig. 2 which are actually observed in real systems, and estimate the spin relaxation rate using the multi-orbital tight-binding model. There we show that the spin-polarized valence bands at K and K' are actually not pure spin states but includes small components of the opposite spin due to the spin-orbit interaction, and this enables the inter-valley scattering under the non-magnetic defects. In the monolayer TMD, such a spin hybridization is relatively weak because of the limitation by the mirror reflection symmetry σ_h, leading to a extremely small spin relaxation rate (long spin relaxation time) compared to the momentum relaxation rate. In the bilayer TMD, on the other hand, the spins are more strongly hybridized due to the absence of the mirror reflection symmetry, and as result, the spin relaxation rate is shown to be greater than in monolayer by the factor of 10^3.

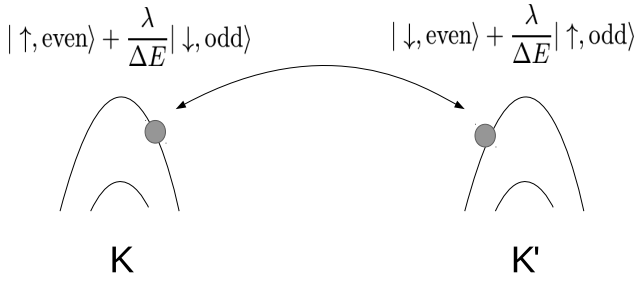

FIG. 1. Schematic description of the inter-valley spin scattering in monolayer TMD.

In TMDs, the electric states around the Fermi energy consists of the d-orbitals ($d_{3r^2-z^2}, d_{x^2-y^2}, d_{xy}, d_{xz}, d_{yz}$) on transition-metal atoms (M = Mo, W) and the p-orbitals (p_x, p_y, p_z) on chalcogen atoms (X = S, Se, Te). As the primitive unit cell contains a single transition-metal atom and two chalcogen atoms, we consider eleven atomic orbitals for each spin in a unit cell. The monolayer TMD has the mirror reflection symmetry σ_h with respect to the layer plane, and therefore the atomic orbitals can be classified into even orbitals ($d_{3z^2-r^2}, d_{x^2-y^2}, d_{xy}, p_x^+, p_y^+, p_z^-$), and odd orbitals ($d_{xz}, d_{yz}, p_x^-, p_y^-, p_z^+$), with respect to the eigenvalue in

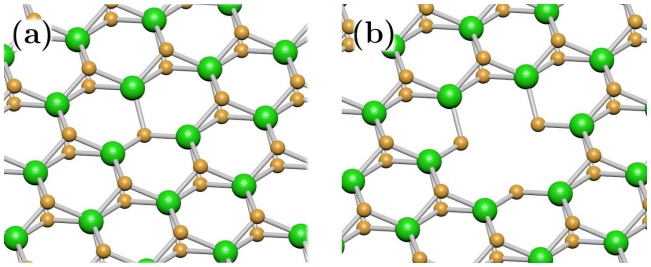

FIG. 2. Atomic structure of (a) a single chalcogen-site vacancy ($V_{\rm X}$), and (b) multiple vacancies on a transition-metal sites and three chalcogen sites ($V_{\rm MX_3}$), in monolayer MX_2.

inverting the z-direction (out-of-plane direction). Here $p_\mu^\pm = p_\mu^{\rm t} \pm p_\mu^{\rm b}$ is the superposition of the atomic orbitals on the vertically located pair of two chalcogen p-orbitals with $p_\mu^{\rm t}$ and $p_\mu^{\rm b}$ for top and bottom. In the absence of the spin-orbit interaction, the even and odd orbitals independently form the even and odd energy bands, respectively. Fig. 3 shows the band structure of MoS_2 calculated by the first-principle method of quantum-ESSPRESSO[29].

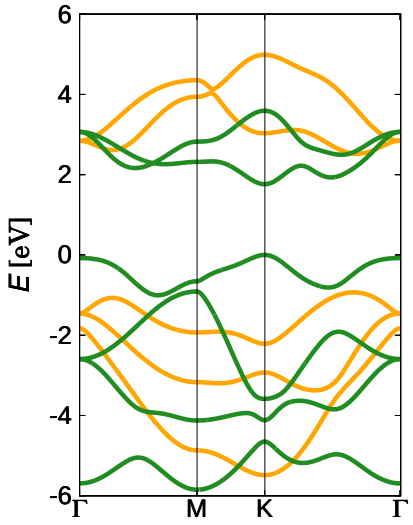

FIG. 3. Band structure of monolayer MoS_2 without spin-orbit interaction. Even and odd bands are indicated by green (dark-colored) and orange (light-colored) curves, respectively.

To describe the motion of electrons, we derive the tight-binding model from the first principle band structure by using Wannier90, which is a numerical package for minimized wannnier functions[30]. We first create the tight-binding Hamiltonian disregarding the spin-orbit interaction, and then introduce $\boldsymbol{L}\cdot\boldsymbol{s}$ spin-orbit term to the transition metal atoms. The Hamiltonian for the spin-independent part is written as

$$H_0 = \sum_{i,j,s} \boldsymbol{a}_i^{s\dagger} t^{\rm e}(i,j)\boldsymbol{a}_j^s + \boldsymbol{b}_i^{s\dagger} t^{\rm o}(i,j)\boldsymbol{b}_j^s \qquad (1)$$

where $\boldsymbol{a}_i^s$ and $\boldsymbol{b}_i^s$ are the annihilation operators for the six even orbitals and the five odd orbitals in the unit cell i, respectively, and with $s = \pm$ represent the spin degree of freedom. The spin-orbit interaction for the d-orbitals of transition-metal atom is described in the basis of $(d_{3z^2-r^2},\, d_{x^2-y^2},\, d_{xy},\, d_{xz},\, d_{yz})$ as[31,32]

$$\tilde{H}_{\rm SO} = \frac{i\lambda}{2}\left(\begin{array}{ccc|cc} 0 & 0 & 0 & -\sqrt{3}\sigma_y & \sqrt{3}\sigma_x \\ 0 & 0 & -2\sigma_z & \sigma_y & \sigma_x \\ 0 & 2\sigma_z & 0 & -\sigma_x & \sigma_y \\ \hline \sqrt{3}\sigma_y & -\sigma_y & \sigma_x & 0 & -\sigma_z \\ -\sqrt{3}\sigma_x & -\sigma_x & -\sigma_y & \sigma_z & 0 \end{array}\right), \qquad (2)$$

Here the first three orbitals $(d_{3z^2-r^2},\, d_{x^2-y^2},\, d_{xy})$ are even and the latter two $(d_{xz},\, d_{yz})$ are odd under the mirror reflection σ_h. Since the spin flipping terms (σ_x and σ_y) always appear in the off diagonal block connecting even and odd orbitals, the spin orbit Hamiltonian can be written by

$$H_{\rm SO} = \sum_{s,i} \boldsymbol{a}_i^{s\dagger} u^{\rm e}(s)\boldsymbol{a}_i^s + \boldsymbol{b}_i^{s\dagger} u^{\rm o}(s)\boldsymbol{b}_i^s + \left[\boldsymbol{a}_{\boldsymbol{u}_i}^{s\ \dagger} u^{\rm off}(s,\bar{s})\boldsymbol{b}_{\boldsymbol{u}_j}^{\bar{s}} + {\rm h.c}\right], \qquad (3)$$

where $\bar{s}$ represents the opposite spin to s, $u^{\rm e}$ and $u^{\rm o}$ represent the diagonal blocks for even and odd states, respectively, and $u^{\rm off}$ is the off-diagonal block. We neglect the spin-orbit interaction in the chalcogenide atom which is much smaller than that in the transition-metal atom.

Before the detailed numerical calculation, we consider the mechanism of the spin-relaxation through the intervalley scattering in the hole-doped TMD monolayer. It is similar to the conventional Elliot-Yafet process, while the even-odd classification due to the reflection symmetry imposes a limitation to possible scattering process. In TMD, the low-energy spectrum near the band gap is dominated by the even-orbital bands. The diagonal part of $H_{\rm SO}$ is responsible for the band splitting between spin-up and spin-down branches due to $\pm\sigma_z$ terms[1]. As schematically shown in Fig. 1, the valence bands are spin-split in opposite directions between two valleys due to the time-reversal symmetry, and in the moderate hole-doped regime considered in the following, the Fermi energy crosses only $(K,\uparrow)$ and $(K',\downarrow)$ branches.

The off-diagonal part of $H_{\rm SO}$ hybridizes these low-energy even-state bands with the odd-state bands far from the Fermi energy with the opposite spin. The states near K and K' points are then expressed in the first-order perturbation as

$$|K,\uparrow\rangle \approx |{\rm even},\uparrow\rangle + \frac{\Lambda}{\Delta E}|{\rm odd},\downarrow\rangle$$
$$|K',\downarrow\rangle \approx |{\rm even},\downarrow\rangle + \frac{\Lambda}{\Delta E}|{\rm odd},\uparrow\rangle, \qquad (4)$$

where $|{\rm even(odd)},s\rangle$ represents the eigenstate in the absence of spin-orbit coupling, which is a direct product of the even (odd) orbital state and the pure spin state with s. Here Λ is the energy scale of the coupling matrix elements, and ΔE is the typical energy distance from

the Fermi energy to the odd state bands. We can show that Λ vanishes right at K and K' points[26], and linearly increases as the wave number is shifted from the valley center. Apart from the numerical factor (of the order of 1), it is roughly written as

$$\Lambda \sim \lambda k a, \tag{5}$$

where λ is the spin-orbit coupling constant in Eq. (2), k is the relative wave-vector from K or K' (omitted in Eq. (4)), and a is the atomic scale constant. Fig. 4 shows the relative amplitude of spin-down component included in the up-spin state in MoS_2 monolayer (indicated by red dots), which is averaged over the Fermi surface and plotted against the corresponding hole density n_h. We see the amplitude is roughly proportional to $\sqrt{n_h} \propto k$ in consistent with Eq. (5).

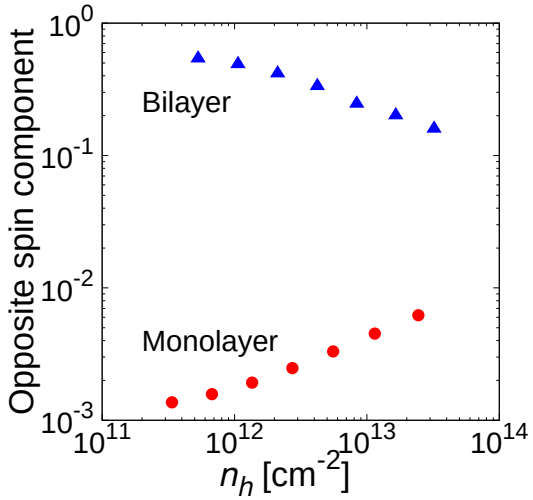

FIG. 4. Relative amplitude of spin-down component included in the up-spin state in MoS_2 monolayer and bilayer, as function of the hole density n_h.

We assume the scatterer H_i is non-magnetic and does not flip spins. Then the scattering matrix element between $|K,\uparrow\rangle$ and $|K',\downarrow\rangle$ is written as

$$\langle K',\downarrow|H_i|K,\uparrow\rangle = \frac{\Lambda}{\Delta E}[\langle \mathrm{odd},\uparrow|H_i|\mathrm{even},\uparrow\rangle + \langle \mathrm{even},\downarrow|H_i|\mathrm{odd},\downarrow\rangle]. \tag{6}$$

We see that H_i is required to break the mirror reflection symmetry to hybridize the odd and even orbital states. If we consider an atomic-scale scattering potential breaking mirror symmetry, we roughly have $\langle \mathrm{even}, s|H_i|\mathrm{odd}, s\rangle \sim Va^2/S$, where V is the energy scale of the potential and S is the total system area. As a result, the inter-valley matrix element can be estimated as

$$\langle K'\downarrow|H_i|K\uparrow\rangle \sim V\frac{\Lambda}{\Delta E}\frac{a^2}{S} \tag{7}$$

When V is small and the scatterers are distributed sparsely in the system with a number density n_i, the inter-valley spin relaxation rate (inverse spin relaxation time) is

$$\Gamma_\mathrm{s} \sim 2\pi|\langle K'\downarrow|H_i|K\uparrow\rangle|^2 n_i \rho S^2, \tag{8}$$

where ρ is the density of states at the Fermi energy per valley and per area.

On the other hand, the momentum scattering rate is dominated by the intra-valley scattering process without spin flip, and it is written as

$$\Gamma_\mathrm{p} \sim 2\pi|\langle K\uparrow|H_i|K\uparrow\rangle|^2 n_i \rho S^2, \tag{9}$$

where $\langle K\uparrow|H_i|K\uparrow\rangle \sim Va^2/S$. The ratio of two scattering rates then becomes

$$\frac{\Gamma_\mathrm{s}}{\Gamma_\mathrm{p}} \sim \left(\frac{\Lambda}{\Delta E}\right)^2 = 2\pi n_h a^2 \frac{\lambda^2}{(\Delta E)^2}, \tag{10}$$

where we used $\Lambda \sim \lambda k_F a$, and $n_h = 2\pi k_F^2/(2\pi)^2$ is the number of holes per unit area. The linear dependence of $\Gamma_\mathrm{s}/\Gamma_\mathrm{p}$ on the hole-density n_h originates from the k-dependence of Λ.

For MoS_2, the strength of the spin-orbit interaction λ is given by $\lambda \approx 0.073$ eV[33], and the odd-even energy distance ΔE is typically 2 eV. The lattice constant is $a \sim 0.3$ nm. At the moderate hole density of $n_h = 10^{12}$ cm^{-2}, for example, the ratio $\Gamma_\mathrm{s}/\Gamma_\mathrm{p}$ becomes 10^{-5}. When assuming the disorder scattering rate $\Gamma_\mathrm{p} \sim 0.01$ eV, for example, we have the spin-relaxation time can be estimated to $\tau_s = \hbar/\Gamma_\mathrm{s} \sim 10$ ns.

The realistic short-ranged scatterers such as atomic defects or vacancies cannot be treated as a perturbational potential, and then we need to actually solve the scattering problem to estimate the spin relaxation rate. We consider two specific mirror-symmetry-breaking configurations which are actually observed in the real materials[28]: a single chalcogen-site vacancy (V_X), and a multiple vacancy on a transition-metal sites and three chalcogen sites (V_{MX_3}), which are shown in Fig. 2 (a) and (b), respectively. We consider a system with a single defect of each type in a tube geometry with a sufficiently large diameter, and calculate the transfer matrix T using the tight-binding model with the one-dimensional transport formula[34].

The scattering rate from the initial state $(s,\boldsymbol{k})$ is given by the T matrix as,

$$\frac{1}{\tau^{\pm}_{s\boldsymbol{k}}} = \frac{2\pi n_i S}{\hbar}\sum_{s'\boldsymbol{k}'}\left|T_{s\boldsymbol{k},s'\boldsymbol{k}'}\right|^2 \delta(\varepsilon_{s\boldsymbol{k}} - \varepsilon_{s'\boldsymbol{k}'})\,\delta_{s',\pm s}, \tag{11}$$

where S is the system area, and τ^+ describes the spin-conserving scattering time and τ^- the spin-flipping scattering time. The momentum relaxation rate and the spin relaxation rate are obtained by

$$\Gamma_\mathrm{p} = \left\langle \frac{1}{\tau^+_{s\boldsymbol{k}}} + \frac{1}{\tau^-_{s\boldsymbol{k}}} \right\rangle_{\varepsilon_F}$$
$$\Gamma_\mathrm{s} = \left\langle \frac{1}{\tau^-_{s\boldsymbol{k}}} \right\rangle_{\varepsilon_F}, \tag{12}$$

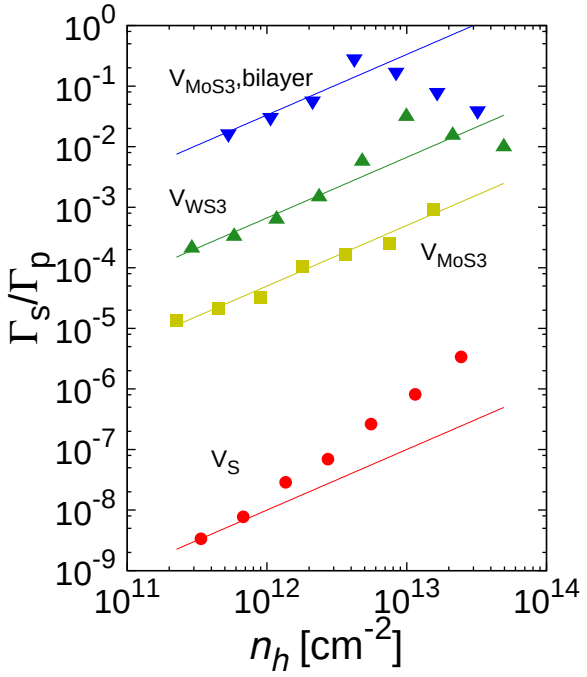

FIG. 5. Relative spin-relaxation rate Γ_s/Γ_p as a function of hole density of n_h, calculated for V_S and V_{MoS_3} in the monolayer MoS_2, V_{WS_3} in the monolayer WS_2. and V_{MoS_3} in the bilayer MoS_2. Solid lines just represent the linear dependence to n_h.

respectively, where $\langle\cdots\rangle_{\varepsilon_F}$ represents the average on the Fermi surface.

First we present the analyses for V_S and V_{MoS_3} in the monolayer MoS_2, and also for V_{WS_3} in the monolayer WS_2. Fig. 5 plots the relative spin-relaxation rate Γ_s/Γ_p averaged on the Fermi surface, as a function of the corresponding hole density n_h. Here Γ_p is found to be always about $n_i a^2$ times a few eV not strongly depending on n_h, so it is reasonable to normalize the spin relaxation rate by Γ_p. For V_{MoS_3} in the monolayer MoS_2, we see that the Γ_s/Γ_p is roughly proportional to n_h in the low density regime, and this is consistent with the qualitative estimation Eq. (10). The absolute value is of the order of 10^{-5} at $n_h \sim 10^{12}$ cm^{-2}, which is also in a good agreement with the estimation. This is somewhat surprising because Eq. (10) was derived in the perturbational approach which is valid in the weak potential limit.

V_{WS_3} in the monolayer WS_2 exhibits a similar behavior, while the absolute value is greater than in MoS_2 about by factor of 10. WS_2 has a larger spin-orbit interaction of $\lambda_{WS_2} \approx 0.211$eV.[33] In Eq. (10), the relative spin-relaxation rate Γ_s/Γ_p is proportional to λ^2, and the order-of-magnitude difference is actually consistent with $(\lambda_{WS_2}/\lambda_{MoS_2})^2 \approx 8.35$. For V_{WS_3}, we see some non-monotonic behavior in higher n_h. This may be related to the impurity bound states, while the detailed study is out of the scope of the present work.

In a simpler defect V_S, the spin relaxation rate is found to be extremely small compared to that of V_{MoS_3}, and it is also deviating from a linear function of n_h. In the low-energy bands, the wave amplitude of the electronic state mainly resides on the transition-metal atoms, and thus a single chalcogen vacancy is expected to have relatively small effect compared to V_{MoS_3}. But it seems not enough to fully explain the difference of the order of a few magnitudes, and we presume some other factor, e.g., cancellation of the leading-order matrix elements, may also contribute to the suppression of the intervalley process.

Finally, we study the spin relaxation rate in the MoS_2 bilayer with a V_{MoS_3} defect. Unlike monolayer, the energy bands in the bilayer TMD are all spin degenerate due to the coexistence of time reversal symmetry and spatial inversion symmetry.[1] However, each eigenstate cannot be expressed as a single spin state because the spin-orbit interaction strongly hybridizes the different spin components in the multiple orbitals. To define the spin relaxation rate using Eq. (11) in this situation, we reconstruct the degenerate Bloch states at each Bloch momentum into approximate "spin-up" and "spin-down" states so as to maximize the expectation value of σ_z. The relative amplitude of the spin-down components in the "spin-up" state in bilayer MoS_2 is shown in Fig. 4, where we still see a strong hybridization about a few of 0.1. In the monolayer, in contrast, the spin hybridization is extremely weak as we have already seen, and this is because the selection rule imposed by the mirror reflection symmetry allows the spin mixing only between the low-energy even bands and the high-energy odd bands. In bilayer, the mirror reflection symmetry is absent and there the spin-orbit interaction directly couples the opposite spin states in the same low-energy bands, giving a strong spin hybridization. The spin relaxation rate Γ_s/Γ_p calculated for bilayer MoS_2 is plotted in Fig. 5, and it is much greater than that of monolayer by the factor of 10^3 reflecting the strong spin mixing effect.

To conclude, we studied the electronic spin relaxation in hole-doped TMD monolayer and bilayer in the presence of realistic atomic defects. By analyzing the band structure and spin-orbit interaction, we qualitatively describe the spin relaxation mechanism and actually estimated the spin-relaxation rate for several specific cases in the numerical calculations. In the monolayer TMD, the inter-band spin hybridization is suppressed by the parity-selection rule under the mirror symmetry, resulting in a relatively smaller spin relaxation rate. The bilayer TMD has a much greater spin relaxation rate in contrast, because of the strong spin hybridization in the absence of the mirror symmetry.

This work was supported by Grants-in-Aid for Scientific research (Grants No. 25107005).

[1] D. Xiao, G.-B. Liu, W. Feng, X. Xu, and W. Yao, Phys. Rev. Lett. **108**, 196802 (2012).
[2] T. Cao, G. Wang, W. Han, H. Ye, C. Zhu, J. Shi, Q. Niu, P. Tan, E. Wang, B. Liu, and J. Feng, Nature Commun. **3**, 887 (2012).
[3] H. Zeng, J. Dai, W. Yao, D. Xiao, and X. Cui, Nat. Nano. **7**, 490 (2012).
[4] K. F. Mak, K. He, J. Shan, and T. F. Heinz, Nat. Nano. **7**, 494 (2012).
[5] H. Shi, H. Pan, Y.-W. Zhang, and B. I. Yakobson, Phys. Rev. B **87**, 155304 (2013).
[6] A. Molina-Sánchez, D. Sangalli, K. Hummer, A. Marini, and L. Wirtz, Phys. Rev. B **88**, 045412 (2013).
[7] R. Suzuki, M. Sakano, Y. J. Zhang, R. Akashi, D. Morikawa, A. Harasawa, K. Yaji, K. Kuroda, K. Miyamoto, T. Okuda, K. Ishizaka, R. Arita, and Y. Iwasa, Nat. Nano. **9**, 611 (2014).
[8] C. Zhang, H. Wang, W. Chan, C. Manolatou, and F. Rana, Phys. Rev. B **89**, 205436 (2014).
[9] M. Yamamoto, S. T. Wang, M. Ni, Y.-F. Lin, S.-L. Li, S. Aikawa, W.-B. Jian, K. Ueno, K. Wakabayashi, and K. Tsukagoshi, ACS Nano **8**, 3895 (2014).
[10] Y. Song and H. Dery, Phys. Rev. Lett. **111**, 026601 (2013).
[11] H. Yuan, X. Wang, B. Lian, H. Zhang, X. Fang, B. Shen, G. Xu, Y. Xu, S.-C. Zhang, H. Y. Hwang, and Y. Cui, Nat. Nano. **advance online publication** (2014), 10.1038/nnano.2014.183.
[12] W. Feng, Y. Yao, W. Zhu, J. Zhou, W. Yao, and D. Xiao, Phys. Rev. B **86**, 165108 (2012).
[13] J. Klinovaja and D. Loss, Phys. Rev. B **88**, 075404 (2013).
[14] A. Kormányos, V. Zólyomi, N. D. Drummond, and G. Burkard, Phys. Rev. X **4**, 011034 (2014).
[15] L. Peng, K. Yao, S. Zhu, Y. Ni, F. Zu, S. Wang, B. Guo, and Y. Tian, J. Appl. Phys. **115**, 223705 (2014).
[16] T. Habe and M. Koshino, arXiv:1411.3088 (2014).
[17] M. I. D'yakonov and V. I. Perel, Sov. Phys. JETP **33**, 1053 (1971).
[18] R. . J. Elliott, Phys. Rev. **96**, 266 (1954).
[19] A. A. Kiselev and K. W. Kim, Phys. Rev. B **61**, 13115 (2000).
[20] T. Kaneko, M. Koshino, and T. Ando, Phys. Rev. B **78**, 245303 (2008).
[21] K. F. Mak, K. He, J. Shan, and T. F. Heinz, Nat Nano **7**, 494 (2012).
[22] L. Wang and M. W. Wu, Phys. Rev. B **89**, 115302 (2014).
[23] L. Wang and M. W. Wu, Phys. Rev. B **89**, 205401 (2014).
[24] H. Ochoa and R. Roldán, Phys. Rev. B **87**, 245421 (2013).
[25] H. Ochoa, F. Guinea, and V. I. Fal'ko, Phys. Rev. B **88**, 195417 (2013).
[26] H. Ochoa, F. Finocchiaro, F. Guinea, and V. I. Fal'ko, Phys. Rev. B **90**, 235429 (2014).
[27] W.-Y. Shan, H.-Z. Lu, and D. Xiao, Phys. Rev. B **88**, 125301 (2013).
[28] W. Zhou, X. Zou, S. Najmaei, Z. Liu, Y. Shi, J. Kong, J. Lou, P. M. Ajayan, B. I. Yakobson, and J.-C. Idrobo, Nano Lett. **13**, 2615 (2013).
[29] P. Giannozzi, S. Baroni, N. Bonini, M. Calandra, R. Car, C. Cavazzoni, D. Ceresoli, G. L. Chiarotti, M. Cococcioni, I. Dabo, A. Dal Corso, S. de Gironcoli, S. Fabris, G. Fratesi, R. Gebauer, U. Gerstmann, C. Gougoussis, A. Kokalj, M. Lazzeri, L. Martin-Samos, N. Marzari, F. Mauri, R. Mazzarello, S. Paolini, A. Pasquarello, L. Paulatto, C. Sbraccia, S. Scandolo, G. Sclauzero, A. P. Seitsonen, A. Smogunov, P. Umari, and R. M. Wentzcovitch, J. Phys.: Condens. Matter **21**, 395502 (2009).
[30] A. A. Mostofi, J. R. Yates, Y.-S. Lee, I. Souza, D. Vanderbilt, and N. Marzari, Computer Physics Communications **178**, 685 (2008).
[31] E. U. Condon and G. H. Shortley, *The Theory of Atomic Spectra* (Cambridge University Press, New york, 1935).
[32] K. V. Shanavas, Z. S. Popović, and S. Satpathy, Phys. Rev. B **90**, 165108 (2014).
[33] G.-B. Liu, W.-Y. Shan, Y. Yao, W. Yao, and D. Xiao, Phys. Rev. B **88**, 085433 (2013).
[34] T. Ando, Phys. Rev. B **44**, 8017 (1991).